Observation of the antiferroquadrupolar order in DyB₂C₂ by resonant x-ray scattering

T. Matsumura, N. Oumi, and K. Hirota
Department of Physics, Tohoku University, Sendai, 980-8578, Japan

H. Nakao and Y. Murakami*
Photon Factory, Institute of Materials Structure Science, High Energy Accelerator Research Organization, Tsukuba, 305-0801, Japan

Y. Wakabayashi†
Department of Physics, Faculty of Science and Technology, Keio University, 3-14-1 Hiyoshi, Yokohama, 223-8522, Japan

T. Arima
Institute of Materials Science, University of Tsukuba, Tsukuba, 305-8573, Japan

S. Ishihara‡ and Y. Endoh
Institute for Materials Research, Tohoku University, Sendai, 980-8577, Japan

We have investigated the antiferroquadrupolar (AFQ) order in DyB₂C₂ by resonant x-ray scattering. X rays with energies near the L_3 absorption edge of Dy were employed. Superlattice peaks that correspond to three kinds of propagation vectors of (1 0 0), (1 0 1/2), and (0 0 1/2) were investigated in detail with polarization analyses. The experimental results are analyzed using a formalism of resonant x-ray scattering and a model of the AFQ order. The magnetic and quadrupolar scatterings are explained by the model satisfactorily. A detailed investigation of the critical behavior of the AFQ ordering is also reported. The critical exponent β is deduced to be 0.35, not far from the three-dimensional Heisenberg system. We have also succeeded in detecting the diffuse scattering above T_Q.

I. INTRODUCTION

There is a class of magnetic materials in which the orbital degree of freedom remains due to highly symmetrical crystalline electric fields (CEF's). Many of such materials undergo phase transitions resulting in the lifting of the orbital degeneracy. In *f*-electron systems, when the CEF ground state has a non-Kramers-type degeneracy, there is a possibility that a periodic ordering of the anisotropic charge distributions of the *f* electrons takes place, other than magnetic orderings. This asphericity can be represented in the lowest order by the quadrupolar moment of the localized *f* electrons. The orderings are driven by quadrupolar pair interactions in combination with magnetoelastic interactions.[1] Even in materials in which magnetic interactions dominate, there are many cases where the magnetic properties are largely influenced by underlying quadrupolar interactions.[2] To study the mechanism of these phenomena the observation of quadrupolar moments, with changing sample environments such as temperature, pressure, and magnetic field, is necessary.

In order to observe the asphericity of charge distribution of an ion, the diffraction method is essential, especially for antiferroquadrupolar (AFQ) orders which normally do not accompany measurable uniform lattice distortions. Various methods using x rays and neutrons have been studied. The most direct way to observe the asphericity of an electron shell is to use x-ray Thomson scattering in the nonresonant region. Keating's experiment on holmium succeeded in detecting the scattering of x rays from the spiral arrangement of aspherical 4*f* shells occurring at twice the magnetic propa-

gation vector.[3] The same method was formulated by Amara and Morin using multipole expansion, giving a description of the scattering in terms of quadrupolar moments of ions.[4] The AFQ order in NdMg was observed successfully.[5] We also refer to an x-ray powder-diffraction combined with maximum entropy method which succeeded in drawing a charge density map of a manganese oxide in an orbital-ordered phase.[6]

Neutron scattering can also be used to study the quadrupolar orders, although neutrons do not have a direct coupling with electric charges. Measurement of magnetic form factors can give information on aspherical charge distributions through spin densities. The first observation was performed by Ito and Akimitsu for K₂CuF₄.[7,8] Felcher *et al.* measured the scattering-vector dependence and the temperature dependence of the aspherical part of the magnetic form factor, i.e., the $\langle j_2 \rangle$ term, of holmium by observing the third harmonic of the magnetic Bragg peak.[9] In CeB₆ and TmTe, the existence of the AFQ phase with no magnetic order has been established through measurements of the induced antiferromagnetic (AFM) moments in magnetic fields.[10–14] Since the directions of the induced magnetic moments are coupled with the underlying quadrupolar moments, the quadrupolar order parameter can be estimated from symmetry arguments.[15] However, both the form-factor measurement and the induced-moment measurement require a magnetic field, which changes the unperturbed state in zero field.

An appropriate method for each substance and purpose has been employed. In holmium, since it shows ideally the spiral magnetic structure, measurement of higher harmonics

is directly connected to the aspherical component. Then the detailed measurement of the temperature dependence of the aspherical component by neutron scattering in zero magnetic field was possible.[9] This is not the case for high-symmetry systems like NdMg, CeB_6, and TmTe. We need to rely on x-ray scattering if we want to detect quadrupolar order in zero field, unless the sample exhibits periodic lattice distortion which is detectable with neutrons as in UPd_3.[16] A great advantage of nonresonant x-ray scattering is that we can obtain the absolute value of the ordered quadrupolar moment. However, the count rate could be so weak and it might be difficult to collect detailed data with changing sample environments.[4,5] In CeB_6 and TmTe, x-ray scattering experiments have been very difficult because of their low transition temperatures for x-ray experiments: $T_Q = 3.3$ K for CeB_6 and 1.8 K for TmTe. Further, no indications of periodic lattice distortion have been observed for the two compounds. Then the induced AFM structures in magnetic fields have been the clearest experimental evidence for the AFQ orders. Recently, superlattice reflections of (1/2 1/2 1/2) have been observed in CeB_6 by resonant x-ray scattering that provide important pieces of information for the problem of AFQ order.[17,18] Finally, form-factor measurements using x rays and neutrons combined with a Fourier analysis or maximum entropy method are quite effective when we want to investigate actual images of spin or charge distributions in real space. However, these are not suitable for the measurement of order parameters with changing sample environments.

The purpose of the present study is to observe the quadrupolar and magnetic order parameters of a rare-earth compound DyB_2C_2 in zero magnetic field. We have employed resonant x-ray scattering for this purpose, which has recently been applied to observations of orbital orders in $3d$ transition-metal oxides.[19,20] This method utilizes the characteristic that an atomic scattering factor is largely enhanced when the energy of an x ray is tuned at an absorption edge of the atom. The first advantage of this method is the high count rate due to the enhancement at the absorption edge. This makes it possible to measure temperature, azimuthal angle, polarization, and energy dependences of the peak intensities in detail.[21] Second, element selectivity guarantees that the resonant peak arises only from the element in study without doubt. Third, we can distinguish a periodic arrangement of the quadrupolar moments from periodic lattice distortions by measuring the energy dependence of the superlattice peak. Finally, the experiment can be performed with a small piece of single crystal using natural boron, which makes neutron scattering experiments difficult. A disadvantage is first that this method is not as direct as nonresonant x-ray Thomson scattering; it is not possible to deduce the absolute value of the moment. Second, the scattering mechanism has not yet been solidly established. Several scattering mechanisms in the orbital-ordered state are proposed from different viewpoints, particularly in $3d$ compounds.[22–27] In the present study we simply assume that the $5d$ state is most influenced by the local $4f$ electrons through the Coulomb and exchange interactions, which we believe is the natural interpretation of the resonance in $4f$-electron systems. We will analyze the
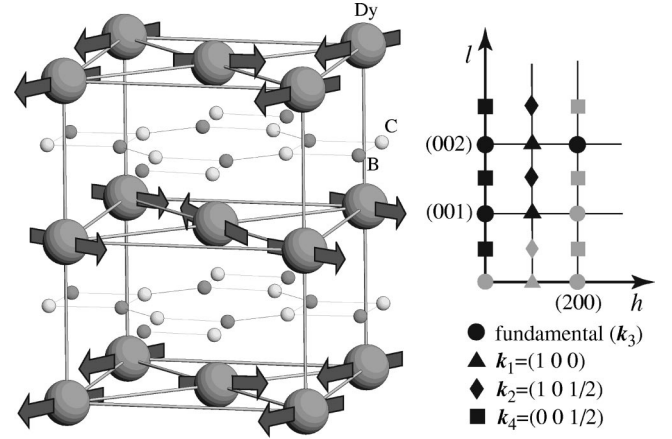

FIG. 1. (left) Crystal structure of DyB_2C_2 ($P4/mbm$, $a = 5.341$ Å, $c = 3.547$ Å at 30 K). The magnetic structure is indicated by the arrows. (right) The h-l plane of the reciprocal space. Black marks are the reflection points that were actually investigated in the present experiment.

data quantitatively using the formulations developed by Blume.[28,29]

DyB_2C_2, with tetragonal LaB_2C_2-type structure, is a compound that has recently been investigated in detail by Yamauchi *et al.* and is considered to show an AFQ order.[30] Two phase transitions are clearly observed at 15 K and at 25 K with an entropy release of $R \ln 2$ and $R \ln 4$, respectively. The three phases are named phase I for $T > 25$ K, phase II for 15 K $< T <$ 25 K, and phase III for $T < 15$ K. No magnetic order appears in phase II. The magnetic order in phase III exhibits an unusual magnetic structure shown in Fig. 1. The structure is represented by the four propagation vectors $k_1 = (100)$, $k_2 = (101/2)$, $k_3 = (000)$, and $k_4 = (001/2)$. The basic magnetic structure, where the magnetic moments on a c plane lie along the $[1\,1\,0]$ directions with those on the neighboring c plane along the $[1\,\bar{1}\,0]$ directions, is described by k_1 and k_2. Canting of the moments from the $[1\,1\,0]$ directions by an angle of 28° is described by k_3 and k_4. These properties can naturally be understood by assuming an underlying AFQ order. The propagation vector of the AFQ order that is consistent with the basic magnetic structure is expected to be (0 0 1/2) if we assume a strong spin-orbit coupling.

The first resonant x-ray scattering experiment on DyB_2C_2 was performed by Hirota *et al.*[31] They discovered two kinds of superlattice reflections of $k_2 = (101/2)$ and $k_4 = (001/2)$ that appear below $T_Q = 25$ K. From incident energy, temperature, azimuthal angle, and polarization dependences, they established that these signals arise from the AFQ order. In particular, the characteristic azimuthal-angle dependences for the σ-σ' ($\propto \sin^2 2\varphi$) and the σ-π' ($\propto \cos^2 2\varphi$) scatterings were considered to reflect the AFQ order of the $4f$ electrons. Another reflection of $k_1 = (100)$ was also found to appear below $T_N = 15$ K only for σ-π' scattering, reflecting the AFM order. Tanaka *et al.* also performed a similar experiment independently, though without polarization analysis, and obtained consistent experimental results.[32]

This paper deals with more comprehensive data and

analysis than the first reports of Refs. 31 and 32. The experimental results will be connected quantitatively with the physical picture of AFQ order using the basic formalism described in Sec. II. Section III describes the experimental procedure. We will show in Sec. IV the experimental results and the analysis in the ordered state. We focus especially on the explanation of the azimuthal-angle and polarization dependences of the (0 0 5/2) reflection, assuming a model of AFQ order. We also analyze scatterings of magnetic origin. The critical phenomenon of the AFQ ordering is another topic in this paper, which is treated in Sec. V.

II. THEORY

In order to analyze our experimental results we use the formalism based on symmetry arguments developed by Blume.[29] We summarize the equations in this section. Since we deal with scattering only in the vicinity of the absorpton edge, we do not consider nonresonant terms. The elastic resonant scattering amplitude including up to an electric quadrupole transition can be written as

$$
A_r = -\frac{e^2}{mc^2}\frac{m\omega_0^3}{\omega}\sum_{\alpha,\beta}\varepsilon'_\beta\varepsilon_\alpha\sum_{n,m}e^{i\boldsymbol{\kappa}\cdot(\boldsymbol{n}+\boldsymbol{d}_m)-W_m}\sum_{a,c}p_a
$$

$$
\times\sum_{\gamma,\delta}\frac{\left\langle a\left|R_m^\beta-\frac{i}{2}Q_m^{\beta\delta}k'_\delta\right|c\right\rangle\left\langle c\left|R_m^\alpha+\frac{i}{2}Q_m^{\alpha\gamma}k_\gamma\right|a\right\rangle}{E_a-E_c+\hbar\omega+i\Gamma/2},
$$

$$(1)$$

where

$$
R_m^\alpha=\sum_{i\in m}r_{i\alpha}, \tag{2}
$$

$$
Q_m^{\alpha\beta}=\sum_{i\in m}r_{i\alpha}r_{i\beta} \tag{3}
$$

are the electric dipole and quadrupole moment operators. $\boldsymbol{k}$ ($\boldsymbol{k}'$) and $\boldsymbol{\varepsilon}$ ($\boldsymbol{\varepsilon}'$) are the wave vector and the polarization vector of the incident (scattered) photon, respectively; α, β, γ, and δ vary over the Cartesian indices x, y, and z. The scattering vector is written by $\boldsymbol{\kappa}=\boldsymbol{k}-\boldsymbol{k}'$. The initial and intermediate states of the sample with energies E_a and E_c are represented by $|a\rangle$ and $|c\rangle$, respectively; $\hbar\omega$ is the energy of the photon and $\hbar\omega_0$ is equal to the energy difference E_c-E_a. $\boldsymbol{n}$ represents the position of the nth unit cell and $\boldsymbol{d}_m$ represents the mth atom in the nth unit cell with the Debye-Waller factor W_m. In Eqs. (2) and (3) the summations are taken over all electrons of the mth atom. p_a is the thermodynamic probability that the sample is in the state $|a\rangle$. We have introduced Γ, the width of the resonance, which corresponds to the lifetime of the intermediate state.

The scattering amplitude for the electric dipole ($E1$) transition is written as

$$
A_{E1}=-\frac{e^2}{mc^2}\frac{m\omega_0^3}{\omega}\sum_{n,m}e^{i\boldsymbol{\kappa}\cdot(\boldsymbol{n}+\boldsymbol{d}_m)-W_m}\sum_{\alpha,\beta}\varepsilon'_\beta\varepsilon_\alpha f_m^{\alpha\beta}, \tag{4}
$$

where $f_m^{\alpha\beta}$ is the atomic scattering factor tensor for the $E1$ transition written by

$$
f_m^{\alpha\beta}=\sum_{a,c}p_a\frac{\langle a|R_m^\beta|c\rangle\langle c|R_m^\alpha|a\rangle}{\hbar\omega-\hbar\omega_0+i\Gamma/2}. \tag{5}
$$

We assume here that there exists a special axis for the mth atom. The axis is defined, for instance, by the magnetic moment, by the quadrupolar moment, or by the local crystalline electric field. If we take this axis as the x axis, the atomic scattering factor can be written as

$$
f=d_0\begin{pmatrix}1&0&0\\0&1&0\\0&0&1\end{pmatrix}+id_1\begin{pmatrix}0&0&0\\0&0&1\\0&-1&0\end{pmatrix}
$$

$$
+d_2\begin{pmatrix}\frac{2}{3}&0&0\\[4pt]0&-\frac{1}{3}&0\\[4pt]0&0&-\frac{1}{3}\end{pmatrix}. \tag{6}
$$

The parameters d_0, d_1, and d_2 are the coefficients for the isotropic, asymmetric, and symmetric parts of the tensor, respectively, including the energy dependence $m\omega_0^3/\omega/(\hbar\omega-\hbar\omega_0+i\Gamma/2)$. The d_1 term arises purely from the magnetic moment. When the atom does not have a magnetic moment, the d_1 term vanishes. The coefficients d_0 and d_2 contain both the magnetic and quadrupolar contributions.

With respect to the scattering amplitude for the electric quadrupole ($E2$) transition, we rewrite Blume's equation in a more appealing form. We use the quadrupolar operators defined by

$$
Q_m^u=\sum_{i\in m}(3z_i^2-r_i^2),
$$

$$
Q_m^v=\sum_{i\in m}\sqrt{3}(x_i^2-y_i^2),
$$

$$
Q_m^\xi=\sum_{i\in m}2\sqrt{3}y_iz_i,
$$

$$
Q_m^\eta=\sum_{i\in m}2\sqrt{3}z_ix_i,
$$

$$
Q_m^\zeta=\sum_{i\in m}2\sqrt{3}x_iy_i. \tag{7}
$$

Then the scattering amplitude for the E2 transition is written as

$$
A_{E2}=-\frac{e^2}{mc^2}\frac{m\omega_0^3}{4\omega}\sum_{n,m}e^{i\boldsymbol{\kappa}\cdot(\boldsymbol{n}+\boldsymbol{d}_m)-W_m}\sum_{\alpha,\beta}K'_\beta K_\alpha g_m^{\alpha\beta}, \tag{8}
$$

where $g_m^{\alpha\beta}$ is the atomic scattering factor tensor for the E2 transition written by

$$g_m^{\alpha\beta}=\sum_{a,c} p_a \frac{\langle a|Q_m^{\beta}|c\rangle\langle c|Q_m^{\alpha}|a\rangle}{\hbar\omega-\hbar\omega_0+i\Gamma/2}. \tag{9}$$

Here the indices α and β vary over u, v, ξ, η, and ζ. The coefficient K is calculated to be

$$K_u=\frac{1}{2}\varepsilon_z k_z,$$

$$K_v=\frac{1}{2\sqrt{3}}(\varepsilon_x k_x-\varepsilon_y k_y),$$

$$K_\xi=\frac{1}{2\sqrt{3}}(\varepsilon_y k_z+\varepsilon_z k_y),$$

$$K_\eta=\frac{1}{2\sqrt{3}}(\varepsilon_z k_x+\varepsilon_x k_y),$$

$$K_\zeta=\frac{1}{2\sqrt{3}}(\varepsilon_x k_y+\varepsilon_y k_x). \tag{10}$$

When we assume a special axis for the mth atom and take this axis as the x axis as in the case of the $E1$ transition, the atomic scattering factor for the $E2$ transition can be written as

$$g=\begin{pmatrix} g_{uu} & g_{uv} & 0 & 0 & 0 \\ g_{uv} & g_{vv} & 0 & 0 & 0 \\ 0 & 0 & g_{\xi\xi} & 0 & 0 \\ 0 & 0 & 0 & g_{\eta\eta} & 0 \\ 0 & 0 & 0 & 0 & g_{\zeta\zeta} \end{pmatrix}$$
$$+\begin{pmatrix} 0 & 0 & \sqrt{3}g_{v\xi} & 0 & 0 \\ 0 & 0 & g_{v\xi} & 0 & 0 \\ -\sqrt{3}g_{v\xi} & -g_{v\xi} & 0 & 0 & 0 \\ 0 & 0 & 0 & 0 & g_{\eta\zeta} \\ 0 & 0 & 0 & -g_{\eta\zeta} & 0 \end{pmatrix}, \tag{11}$$

where

$$g_{uu}=12b_2+4c_2+e_2-8f_2,$$

$$g_{uv}=-\sqrt{3}(4c_2+e_2+4f_2),$$

$$g_{vv}=12b_2+12c_2+3e_2,$$

$$g_{\xi\xi}=12(b_2-f_2),$$

$$g_{\eta\eta}=12(b_2+c_2),$$

$$g_{\zeta\zeta}=12(b_2+c_2), \tag{12}$$

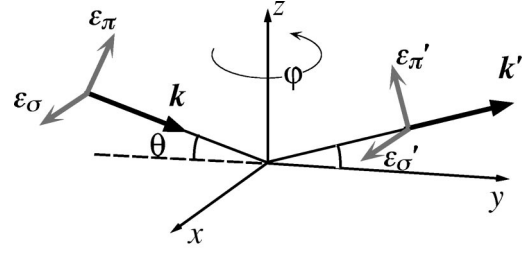FIG. 2. The definition of the vectors associated with the x rays and the axes attatched to the crystal.

and

$$g_{v\xi}=-12ia_1,$$

$$g_{\eta\zeta}=-12i(a_1+b_1). \tag{13}$$

The coefficients b_2, c_2, e_2, and f_2 are for the symmetric part of the scattering factor and a_1 and b_1 are for the asymmetric part, respectively. These are the same coefficients used in Ref. 29 and include the same energy dependence as in the $E1$ transition. The asymmetric part is purely of magnetic origin and the symmetric part contains both magnetic and quadrupolar contributions.

We notice from Eq. (1) that there appears a cross term of dipole and quadrupole transitions. We do not consider this contribution in this paper because the Dy atom is located at the center of symmetry and the cross term vanishes.

The wave vectors and the polarization vectors for the scattering configuration illustrated in Fig. 2 are written as

$$\mathbf{k}=k(0,\cos\theta,-\sin\theta),$$

$$\mathbf{k}'=k(0,\cos\theta,\sin\theta),$$

$$\boldsymbol{\varepsilon}_\sigma=(1,0,0),$$

$$\boldsymbol{\varepsilon}_\pi=(0,\sin\theta,\cos\theta),$$

$$\boldsymbol{\varepsilon}'_\sigma=(1,0,0),$$

$$\boldsymbol{\varepsilon}'_\pi=(0,-\sin\theta,\cos\theta). \tag{14}$$

When the sample is rotated around the z axis by an azimuthal angle φ, the rotation matrix

$$U(\varphi)=\begin{pmatrix} \cos\varphi & \sin\varphi & 0 \\ -\sin\varphi & \cos\varphi & 0 \\ 0 & 0 & 1 \end{pmatrix} \tag{15}$$

must be operated to all of the vectors in Eq. (14) from the left.

III. EXPERIMENT

The crystal was grown by the Czochralski pulling method with a tetra-arc furnace. The obtained single crystal was checked by powder x-ray diffraction, which showed a single-phase pattern of DyB_2C_2. The temperature dependence of the

magnetic susceptibility also agreed with the data reported in Ref. 30.

X-ray scattering measurements were performed on a four-circle diffractometer at BL-16A2 of the Photon Factory in KEK. A sample with a c-plane surface ($\sim 2 \times 2$ mm^2) was mounted in a closed-cycle ^{4}He refrigerator so as to align the c axis parallel to the ϕ axis of the diffractometer; i.e., the c axis is parallel to the z axis in Fig. 2. The mosaic width was 0.09° full width at half maximum (FWHM). The azimuthal angle φ is defined to be zero when the b axis is parallel to the scattering plane. The azimuthal-angle scan can be performed by rotating the ϕ axis of the diffractometer.

The incident x ray is almost linearly polarized with its electric field perpendicular to the scattering plane (σ polarization). The polarization of the diffracted beam, i.e., σ' (perpendicular to the scattering plane) or π' (parallel to the scattering plane), was analyzed using the PG(0 0 6) reflection. The scattering angle of this reflection is about 91° around the L_3 edge of Dy, resulting in almost perfect analysis. The contamination of the π component in the incident x ray was estimated to be 1.5% from the intensity ratio π-π'/σ-σ' of the (0 0 2) fundamental reflection.

IV. ORDERED STATE

A. Experimental results

The investigation of the reflection corresponding to $k_4 = (0\,0\,1/2)$ was performed using the (0 0 5/2) reflection. The incident energy dependence of the intensity at 30 K, 20 K, and 10 K, which correspond to phases I, II, and III, respectively, is shown in Fig. 3. The measured peak top intensities have been transformed into the integrated intensities by multiplying the width so as to be compared with other figures in the same scale. To compare the integrated intensities with the calculated intensities, the data have been corrected for the absorption and for the Lorentz factor; the absorption coefficient was deduced from the fluorescence spectrum.[31,33]

Resonant peaks are clearly observed in the spectra at 10 K and 20 K, while they are not observed at 30 K. The main-edge peak at 7.792 keV corresponds to the resonance due to the $2p \leftrightarrow 5d$ electric dipole transition. The pre-edge peak at 7.782 keV that is well resolved in the σ-π' process is probably attributed to the $2p \leftrightarrow 4f$ electric quadrupole transition. These assignments are consistent with previous experiments on substances including Dy or other rare-earth elements.[33–39] Concerning the σ-σ' process it was not possible to decide if there was any resonance at 7.782 keV because of the wide peak at the main edge. A very small peak was observed at 10 K for the σ-σ' process at $\varphi = 0°$. This result is rather confusing since the peak is located between 7.792 keV and 7.782 keV.

The temperature dependences of the integrated intensities have been measured for each resonant peak in Fig. 3.[31] The resonant peaks which are observed both at 10 K and 20 K appear below $T_Q = 25$ K [Figs. 3(b) and 3(c)], while those which are observed only at 10 K appear below $T_N = 15$ K [Figs. 3(a) and 3(d)]. Then the former peaks can be attributed to quadrupolar origin and the latter to magnetic origin. With
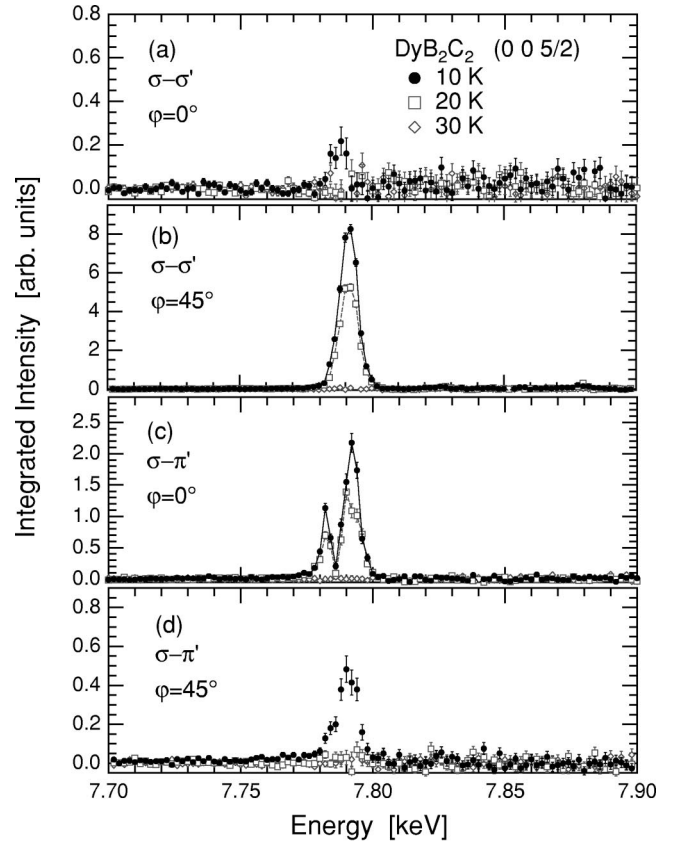

FIG. 3. Incident energy dependences of the integrated intensity of the (0 0 5/2) reflections corrected for the absorption and the Lorentz factor: (a) σ-σ' scattering at $\varphi = 0°$, (b) σ-σ' scattering at $\varphi = 45°$, (c) σ-π' scattering at $\varphi = 0°$, and (d) σ-π' scattering at $\varphi = 45°$. Note that the integrated intensity of the (0 0 2) fundamental peak is 2×10^5.

regard to the main-edge and pre-edge peaks in Fig. 3(c), the intensities at $\varphi = 0°$ exhibit the same temperature dependence.

Figure 4 shows the azimuthal-angle dependences of the integrated intensity at 7.792 keV. The peak profile was measured by a θ-2θ scan for each point and was fit to a Gaussian. The intensity of the σ-σ' process exhibits a $\sin^2 2\varphi$ dependence below T_Q. The intensity of the σ-π' process exhibits a $\cos^2 2\varphi$ dependence at temperatures between T_Q and T_N, and some magnetic contribution is added below T_N. The azimuthal-angle dependence of the pre-edge peak for the σ-π' process is shown in Fig. 5. The intensity exhibits completely the same angle dependence as that of the main edge, i.e., $\propto \cos^2 2\varphi$. With regard to the σ-σ' process, the intensity at 7.782 keV also exhibits the same azimuthal-angle dependence with that at 7.792 keV. However, it was not possible to separate the pre-edge component from the tail of the main-edge peak.

The incident energy dependences of the integrated intensity of the (1 0 2) and (1 0 5/2) reflections, which correspond to k_1 and k_2, respectively, are shown in Fig. 6. The scale of the vertical axis is the same as those of Figs. 3–5. The measurement of the temperature dependence of these resonant peaks shows that they appear below T_N, indicating a mag-
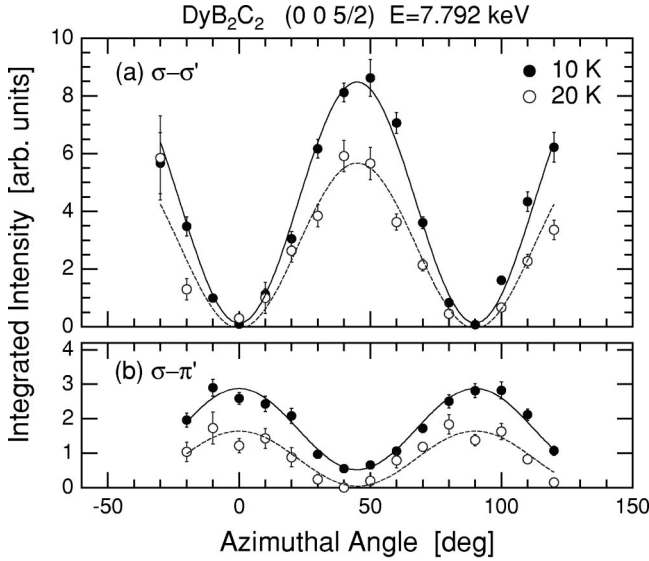
FIG. 4. Azimuthal-angle dependences of the integrated intensity of the (0 0 5/2) reflection for the σ-σ' and the σ-π' scatterings at the main edge. Solid lines are the fits with $\sin^2 2\varphi$ for σ-σ' and with $\cos^2 2\varphi$ for σ-π'.

netic origin. It should be noted that there is a small shoulder at the lower energy side of the main edge, which is more clearly observed in the (1 0 5/2) reflection. This is considered to be of the electric quadrupole transition. With regard to the σ-σ' process, no signal was observed at (1 0 2). On the other hand, the (1 0 5/2) reflection exhibits a nonresonant-type energy dependence which appears below T_Q.[31] This indicates that a periodic lattice distortion occurs simultaneously with the AFQ ordering. This point will be discussed in Sec. VI.

B. Analysis

1. Model calculation

Let us analyze the above experimental results using the formalism described in Sec. II. Figure 7 illustrates a model
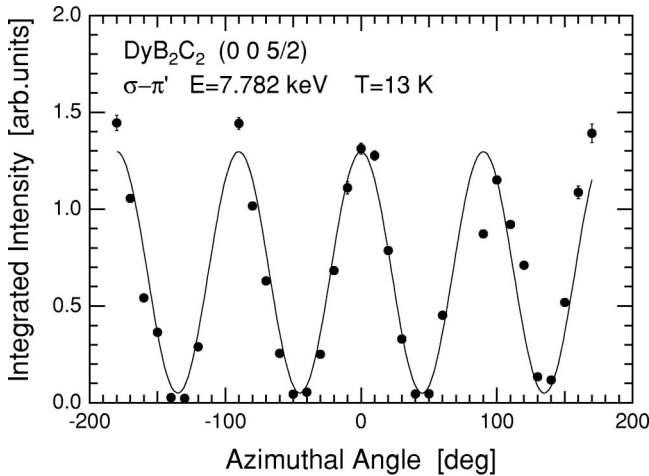
FIG. 5. Azimuthal-angle dependence of the integrated intensity of the (0 0 5/2) reflection for the σ-π' scattering at the pre-edge. The solid line is a fit with $\cos^2 2\varphi$.
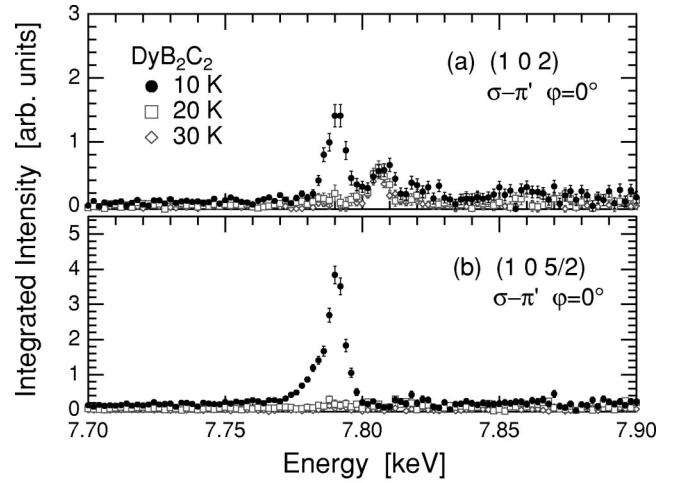
FIG. 6. Incident energy dependences of the integrated intensity for the σ-π' scatterings at $\varphi = 0°$ corrected for the absorption and the Lorentz factor: (a) (1 0 2) reflection and (b) (1 0 5/2) reflection.

of the AFQ order of the $4f$ electrons of the Dy ions, which is expected from the magnetic structure in phase III. We introduce the canting angle α as a parameter. We assume each ion has its own special axis depending on the local quadrupolar or magnetic moment, around which the charge distribution is symmetric. We define the direction of the magnetic moment in phase III as the x axis. Since the spin-orbit coupling is strong, the x axis and the principal axis of the quadrupolar moment coincide. To calculate the scattering amplitudes A_{E1} and A_{E2} at an azimuthal angle φ, it is necessary to rotate the vectors in Eq. (14) so that the xyz axes in Fig. 2 coincide with those in Fig. 7 for each ion; i.e., the rotation of $-\pi/4 + \alpha + \varphi$ for Dy(1), $3\pi/4 - \alpha + \varphi$ for Dy(2), $\pi/4 + \alpha + \varphi$ for Dy(3), and $-3\pi/4 - \alpha + \varphi$ for Dy(4) is performed using Eq. (15).

The resonant scattering cross section is equal to the square of the scattering amplitude A_r. The intensities of the (0 0 5/2) resonant scattering for the electric dipole ($E1$) transition are calculated to be

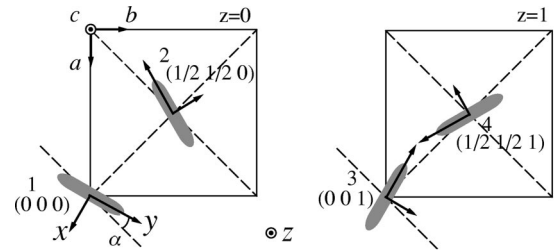$$|A_{k_4,E1}^{\sigma-\sigma'}|^2 \propto |2d_2 \cos 2\alpha \sin 2\varphi|^2, \tag{16}$$

FIG. 7. A model of the antiferroquadrupolar order in DyB$_2$C$_2$. The shadows represent the anisotropic charge distributions. The unit cell is expressed by $a \times a \times 2c$, which contains four Dy ions. The canting angle α from the [1 1 0]-equivalent axes is treated as a parameter. The direction of the magnetic moment in phase III is taken as the x axis.

$$|A_{k_4,E1}^{\sigma-\pi'}|^2 \propto |2d_2 \cos 2\alpha \cos 2\varphi \sin\theta$$

$$+ 2\sqrt{2} i d_1 \sin\alpha \sin\varphi \cos\theta|^2, \qquad (17)$$

and for the electric quadrupole ($E2$) transition,

$$|A_{k_4,E2}^{\sigma-\sigma'}|^2 \propto |2(c_2+f_2)\cos 2\alpha \sin 2\varphi \sin^2\theta$$

$$+ 2i\sqrt{2}\{a_1 + b_1(2\cos 2\alpha \cos 2\varphi + \cos 2\varphi$$

$$- \cos 2\alpha)\}\cos\varphi \sin\alpha \sin 2\theta|^2/16, \qquad (18)$$

$$|A_{k_4,E2}^{\sigma-\pi'}|^2 \propto \left|\frac{1}{2}\{(4c_2+e_2+4f_2)+(4c_2+e_2+4f_2+4c_2\right.$$

$$+ 4f_2)\cos 2\theta\}\cos 2\alpha \cos 2\varphi \sin\theta$$

$$\left.+ i(\text{terms of } a_1 \text{ and } b_1)\right|^2 \Big/ 16. \qquad (19)$$

Second, the intensities of the (1 0 2) resonant scattering at $\varphi=0°$ for the $E1$ transition are calculated to be

$$|A_{k_1,E1}^{\sigma-\sigma'}|^2 \propto 0, \qquad (20)$$

$$|A_{k_1,E1}^{\sigma-\pi'}|^2 \propto |0.63\sqrt{2} i d_1 \sin\theta \cos\alpha|^2, \qquad (21)$$

and for the $E2$ transition,

$$|A_{k_1,E2}^{\sigma-\sigma'}|^2 \propto |(2.7a_1 \cos 2\alpha + 0.94 b_1 \cos 2\alpha$$

$$- 1.2 b_1 \cos 3\alpha)\sin 2\theta|^2/16, \qquad (22)$$

$$|A_{k_1,E2}^{\sigma-\pi'}|^2 \propto |(\text{terms of } a_1, b_1, \text{ and } e_2)|^2/16. \qquad (23)$$

Finally, the scattering intensities of the (1 0 5/2) resonant scattering at $\varphi=0°$ for the $E1$ transition are calculated to be

$$|A_{k_2,E1}^{\sigma-\sigma'}|^2 \propto |1.9 d_2 \sin 2\alpha|^2, \qquad (24)$$

$$|A_{k_2,E1}^{\sigma-\pi'}|^2 \propto |2\sqrt{2} i d_1 \cos\alpha \cos\theta + 0.5 d_2 \sin 2\alpha \cos\theta|^2, \qquad (25)$$

and for the $E2$ transition,

$$|A_{k_2,E2}^{\sigma-\sigma'}|^2 \propto |2\{0.47(c_2+f_2)+0.031 e_2\}\sin 2\alpha \cos 2\theta$$

$$- \{1.1(c_2+f_2)+0.061 e_2\}\sin 2\alpha|^2/16 \qquad (26)$$

$$|A_{k_2,E2}^{\sigma-\pi'}|^2 \propto |(\text{terms of } a_1, b_1, e_2, \text{ and } c_2+f_2)|^2/16. \qquad (27)$$

The factor of $|e^2/mc^2|^2$ has been omitted in the above expressions to save space. The expressions for the $\sigma-\pi'$ process for the $E2$ transition are not written explicitly since there appear many terms; only the parameters which appear are written.

2. Dipole transition

The azimuthal-angle dependences of the (0 0 5/2) reflection at 7.792 keV in Fig. 4 are well reproduced by Eqs. (16) and (17). The $\sin^2 2\varphi$ dependence of the $\sigma-\sigma'$ process and the $\cos^2 2\varphi$ dependence of the $\sigma-\pi'$ process are explained by the d_2 term. Between T_N and T_Q, d_1 vanishes and d_2 arises only from the quadrupolar moment of the $4f$ electrons. The intensity ratio $I^{\sigma-\pi'}/I^{\sigma-\sigma'} \approx 0.3$ can be explained by $\sin^2\theta = 0.3155$ for the Bragg angle of the (0 0 5/2) reflection. The d_1 term contributes below T_N. If we assume $\alpha=28°$ as determined in Ref. 30, we obtain $d_1=(f_{yz}-f_{zy})/2i=0.91$ and $d_2=(f_{xx}-f_{yy})=2.6$ to explain quantitatively the integrated intensities of the (0 0 5/2) reflection at 10 K by Eqs. (16) and (17). By comparing the integrated intensity with that of the (0 0 2) fundamental reflection (2×10^5), which is ascribed to the Thomson scattering from 4×88 electrons, we can deduce that the value of $d_2=2.6$ corresponds to 1.4 electrons (per four molecules).

Below T_N the ordered magnetic moment also contributes to d_2 through an exchange splitting and a spin polarization of the $5d$ level.[34] This should manifest below T_N in the temperature dependence of the intensity. However, the intensity for the $\sigma-\sigma'$ process at $\varphi=45°$ does not show any clear kink in the temperature dependence around T_N. This result indicates that d_2 is caused mostly by the quadrupolar moment through Coulomb interactions between $4f$ and $5d$ electrons. The contribution of the magnetic moment, which is estimated to be $7.1\mu_B$ in Ref. 30, seems much smaller than that of the quadrupolar moment.

Using Eqs. (21) and (25), the above parameters at 10 K, i.e., $\alpha=28°$, $d_1=0.91$, and $d_2=2.6$, give the integrated intensities of 0.11 for the (1 0 2) reflection and 4.17 for the (1 0 5/2) reflection, respectively. The value of 0.11 for the (1 0 2) reflection does not reproduce the experimental result of about 1.5 in Fig. 6. This can be ascribed to the experimental difficulty of rotating the crystal to different reciprocal lattice points without changing the effective volume which contributes to the scattering. However, the calculation at least explains these two magnetic peaks qualitatively.

According to Eq. (17) the intensity of the (0 0 5/2) reflection for the $\sigma-\pi'$ process at $\varphi=45°$ is proportional to $|d_1 \sin\alpha|^2$. The fact that a finite intensity is observed at 10 K indicates that the canting angle of the magnetic moment is certainly not zero below T_N. On the other hand, Eq. (25) shows that the intensity of the (1 0 5/2) reflection for the $\sigma-\pi'$ scattering at $\varphi=0°$ is proportional to $|d_2 \sin 2\alpha|^2$ above T_N since the d_1 term vanishes. The experimental result in Fig. 6 shows that the intensity completely disappears at 20 K. This indicates that the canting angle of the quadrupolar moment could be zero at 20 K since d_2 is definitely not zero at this temperature. Then, it is suggested that the canting of the moments occurs only below T_N.

From Eq. (24) we see that the $\sigma-\sigma'$ scattering of the (1 0 5/2) reflection can also be a measure of the canting angle. However, since this scattering shows a nonresonant-type energy dependence as a result of a periodic lattice distortion,[31] it was difficult to extract the resonant contribution at 7.792

keV with sufficient accuracy to examine the behavior of the canting angle in detail.

3. Quadrupole transition

The calculated results are qualitatively consistent with the experimental results. The azimuthal-angle dependence of the (0 0 5/2) reflection for the σ-π' process at 7.782 keV shown in Fig. 5 is well reproduced by the quadrupolar terms of $4c_2 + e_2 + 4f_2 = -g_{uv}/\sqrt{3}$ and $4(c_2 + f_2) = -(g_{\xi\xi} - g_{\eta\eta})/3$ in Eq. (19). The quadrupolar term of Eq. (18) is also consistent with the experiment. The very small intensities in Figs. 3(a) and 3(d) might be the magnetic signal from a_1 and b_1 terms.

The magnitudes of g_{uv} and $(g_{\xi\xi} - g_{\eta\eta})$ could be estimated by comparing the intensity of the σ-π' process with that of the σ-σ' process. However, we were not able to estimate the pre-edge peak intensity for the σ-σ' process because of the difficulty in resolving the resonant peak into two peaks of $E1$ and $E2$ transitions.

With regard to the σ-π' scattering of the (1 0 2) and (1 0 5/2) reflections, the small shoulders around the pre-edge in Fig. 6 can be ascribed to the magnetic signal due to the a_1 and b_1 terms in Eqs. (23) and (27), respectively. The quadrupolar terms of e_2 and $c_2 + f_2$ have a factor of $\sin 2\alpha$ or $\sin 4\alpha$. Then, the fact that the intensity disappears above T_N is consistent with the argument on the canting angle in the previous subsection.

V. CRITICAL PHENOMENA

Our interest here is to investigate the critical phenomena associated with AFQ ordering by measuring the peak profiles precisely, especially around the transition temperature T_Q. While almost all orbital orderings in manganese oxides exhibit first-order-like phase transitions, AFQ ordering in DyB_2C_2 is considered to be of second order. Information on the critical phenomena may give some insight into the mechanism of the interaction between the quadrupole moments.

We have utilized a Ge (111) crystal as an analyzer to obtain good resolution to observe diffuse scatterings. The longitudinal (0 0 l) scans for both the (0 0 2) fundamental Bragg peak and the well-developed (0 0 5/2) superlattice Bragg peak at low temperature were able to be reproduced by a squared Lorentzian with its FWHM of 0.0011 Å^{-1}. We have therefore assumed this as the resolution function for the present measurement.

We have concentrated in this study on the (0 0 5/2) reflection at $\varphi = 45°$. Although the polarization analysis was not performed, we already know from Fig. 4 that this reflection consists only of σ-σ' scattering above T_N. The measurement was performed much more precisely than the one in Ref. 31. Although the temperature stability of the thermometer was kept within ± 0.01 K, heating of the sample by the beam caused a serious problem in the measurement of the temperature dependence of the weak signals at the critical region. The problem is that the beam intensity changes with the ring current, which decreases typically from 400 mA to
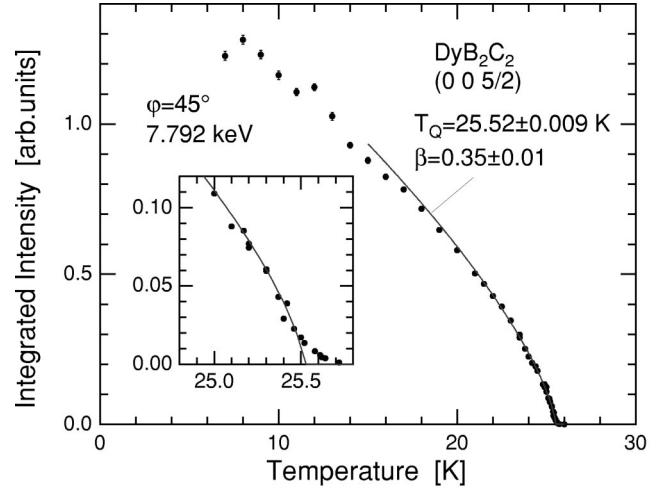

FIG. 8. Temperature dependence of the integrated intensity of the (0 0 5/2) reflection for the (0 0 l) scan at $\varphi = 45°$ measured with a Ge(111) analyzer. The solid line is a fit to a power law $I \propto ((T_Q - T)/T_Q)^{2\beta}$. The inset shows the integrated intensity around the transition temperature.

250 mA in a day. This leads to different heating powers. It reached about 0.25 K at most when the beam intensity was high. Therefore, very careful data taking and treatment of the data—namely, shifting of the temperature—were necessary.

The integrated intensities and the peak widths were obtained by fitting the profiles to a squared Lorentzian. Figure 8 shows the obtained temperature dependence of the integrated intensity of the (0 0 5/2) reflection for the longitudinal (0 0 l) scans. Note that the scale of the vertical axis is different from the other figures. The intensities below T_Q were fitted to a power law $I \propto [(T_Q - T)/T_Q]^{2\beta}$ with varying the fitting range from 15–25.5 K to 23–25.5 K. The obtained parameters are $T_Q = 25.52 \pm 0.009$ K and $\beta = 0.35 \pm 0.01$, which are demonstrated by the solid line in the figure. This β is different from the previously reported value of 0.18 in Ref. 31; this is probably because the previous measurement did not have enough accuracy to determine the critical exponent due to small number of data points.

The inset in Fig. 8 shows the integrated intensity around T_Q. Although a careful data treatment was necessary to estimate the reliable temperatures as described above, it is certain that the intensity does not vanish even above T_Q. An increase in the peak width was also observed around T_Q. The FWHM of the original profile was deconvoluted with the resolution function and was converted to the inverse correlation length along the c axis. The result is shown in Fig. 9. Although κ_c increases with increasing the temperature above T_Q, it was not possible to deduce the critical exponent from these small number of points.

VI. DISCUSSIONS

A. Four propagation vectors

We can interpret the appearance of the four propagation vectors in the following way. At $T_Q = 25$ K the AFQ order with $k_4 = (0\,0\,1/2)$ occurs. The AFQ moment is the principal
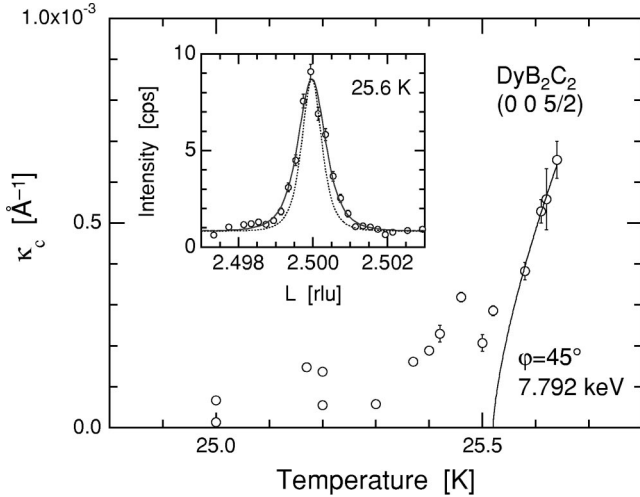
FIG. 9. Temperature dependence of the inverse correlation length along the c axis obtained by deconvoluting the peak widths to the resolution width. The solid line is a calculated curve for the critical exponent $\nu = 0.7$. The inset shows the peak profile at $T = 25.6$ K. The solid line is a fit to a squared Lorentzian and the dotted line is a squared Lorentzian with the same height and with the resolution width.

order parameter and induces a periodic lattice distortion with $k_2 = (1\ 0\ 1/2)$ through some quadrupole-strain couplings. It should be noted that $(1\ 0\ 1/2)$ and $(0\ 0\ 1/2)$ are the equivalent reciprocal lattice points. The resonance can occur also at $(1\ 0\ 1/2)$ simultaneously with the resonance at $(0\ 0\ 1/2)$. However, we could not identify the resonance at $(1\ 0\ 5/2)$ because nonresonant scattering was dominant in the σ-σ' process or because the canting angle of the quadrupolar moment could be zero in phase II.

Below $T_N = 15$ K the AFM order with $k_1 = (1\ 0\ 0)$ occurs. The AFM moment becomes the additional order parameter in this phase. Since $(1\ 0\ 0)$ and $(0\ 0\ 0)$ are the equivalent reciprocal lattice points, the magnetic Bragg peak also appears at $k_3 = (0\ 0\ 0)$. Furthermore, since there is already an AFQ order which confines the direction of the magnetic moments, the resultant magnetic structure also gives magnetic Bragg peaks at $(1\ 0\ 1/2)$ and at $(0\ 0\ 1/2)$. Thus, the four propagation vectors are coupled to each other.

B. Periodic displacement of atoms

The nonresonant scattering of the $(1\ 0\ 1/2)$ reflection that appears below T_Q indicates a periodic displacement of the atoms, which leads to a Bragg reflection due to Thomson scattering. Tanaka *et al.* interpreted this reflection as a displacement of B and C atoms which reduces the symmetry to the space group $P4_2/mnm$.[32] Lovesey and Knight recently gave a theoretical calculation,[40] in which they explained the $(0\ 0\ 1/2)$ resonant peak from the same standpoint as in Ref. 32. However, we consider that the displacement of B and C atoms is not realistic because the estimated scattering factors of the possible reflections from such structure are not consistent with experimental results. If we assume the z parameter of the $8j$ site of $P4_2/mnm$, where the B and C atoms are

located, shifted from the original value of 0.5 to 0.45, the squared structure factor for the $(1\ 0\ 5/2)$ reflection becomes only 0.0376 whereas those for $(1\ 1\ 3/2)$ and $(2\ 2\ 3/2)$ become 154.6 and 170.6, respectively. Therefore, much stronger reflections are expected for the two points. However, none of these reflections have been observed. Furthermore, neutron powder diffraction experiments also do not show any evidence of the displacement of B and C atoms.[41]

Since the atomic scattering factor of a Dy ion is much larger than that of B and C, it is natural to attribute the nonresonant $(1\ 0\ 1/2)$ reflection to a periodic displacement of the Dy ions. We propose a model where the Dy(1) and Dy(4) in Fig. 7 are displaced by $+\delta$ along the c axis and the Dy(2) and Dy(3) by $-\delta$. This gives a superlattice reflection at $(1\ 0\ 1/2)$. The structure factor for the $(1\ 0\ 5/2)$ reflection is calculated to be $F = -4if_{Dy}\sin 5\pi\delta/c$, while that for the $(0\ 0\ 2)$ fundamental reflection is $8f_B + 8f_C + 4f_{Dy}\cos 4\pi\delta/c$. From the observed intensity ratio between $(1\ 0\ 5/2)$ and $(0\ 0\ 2)$, a reasonable value of $\delta/c \approx 4 \times 10^{-4}$ is deduced.

We consider this displacement to be related to the characteristic crystal structure, where the Dy ions are located between the hard B-C layers. This displacement corresponds to one of the 30 phonon modes of DyB_2C_2 at $k = (0\ 0\ 1/2)$. Though there are many other phonon modes that involve displacements of B and C, including the one proposed in Ref. 32, their energy must be very high because they have to modify the strong covalent bonding among the B-C network. On the contrary, the energy scale of the motion of the Dy ions is expected to be small. Then, the position of the Dy ions is considered to be susceptible to quadrupolar orderings through a coupling with the lattice.

There is another reason that the resonant scattering in DyB_2C_2 reflects the AFQ order itself rather than the symmetry of the crystal as in the Templeton scattering.[42] The local symmetries of Dy(1) and Dy(2), as numbered in Fig. 7, are different even in the original crystal structure above T_Q. This can give the $(1\ 0\ 0)$ resonant scattering even above T_Q, which is not observed experimentally. Then, even though there was any displacement of B and C atoms, the effect on the resonant scattering would be negligible. In addition, the displacement of the Dy ions as we propose is a mere 4×10^{-4}, also negligibly small to give any effect on the resonant scattering. Finally, it should be noted that the theory in Ref. 40 can also be applied to our model of AFQ order without the displacement of B and C but with the same space group $P4_2/mnm$; since the theory is based only on the local symmetry of Dy, it is not restricted by the mechanism of symmetry lowering.

C. Critical phenomena

It has been clarified from the present experiment that the order parameter vanishes continuously through T_Q and that there is still a nonvanishing intensity even above T_Q. The temperature dependence of the order parameter below T_Q well follows a normal power law with a critical exponent $\beta = 0.35 \pm 0.01$, which is not an anomalous value when compared with the three-dimensional (3D) Heisenberg model (0.365),[42] 3D XY model (0.345),[42] and actual magnetic sys-

tems such as EuO (0.36) (Ref. 43) and MnF_2 (0.31).[44] These results indicate that the AFQ ordering in DyB_2C_2 is really a second-order phase transition. Note that we assume in this paper that the intensity of the resonant scattering is proportional to the square of the order parameter. Ishihara and Maekawa discuss this relation in Ref. 27.

Concerning the diffuse scattering, it was very difficult to measure precisely the broadening of the width with increasing temperature due to the weak intensity in comparison with the background. However, it should be noted that this result does not directly mean the absence of diffuse scattering. The present situation seems very similar to the case of critical magnetic scattering in MnF_2 studied by x-ray scattering.[44] It was also not possible to measure diffuse scattering above $T_N = 67.4$ K due to weak count rates. However, diffuse scattering certainly exists and was measured up to 10 K above T_N by neutron scattering.[45] The width of the neutron scattering profile was 10 times larger than that of the x-ray scattering.[45]

This problem might be related with the so-called two-length-scale problem. There are some systems in which peak profiles of diffuse scatterings above transition temperatures consist of a narrow central peak and a broad one. Detailed studies of this problem using both neutrons and x rays showed that x-ray signals are dominated by narrow components because of their small resolution volume, while broad components manifest in neutron scattering.[46,47] Though the origin of the narrow component has not yet been established, it is interpreted as a near-surface effect that is more sensitive for x rays.[46,47]

The observed inverse correlation length κ_c of DyB_2C_2 above T_Q is about 5×10^{-4} Å^{-1} at a reduced temperature $(T - T_Q)/T_Q = 4 \times 10^{-3}$, which is read from Fig. 9. This value is as large as that of the narrow component of holmium measured by resonant x-ray scattering at the same reduced temperature $(T - T_N)/T_N$.[46] Furthermore, in holmium, broad diffuse scattering with its width 10 times wider than the narrow component of the x ray is certainly observed by neutron scattering.[46] Therefore, we should not conclude that there is no broad diffuse scattering in DyB_2C_2 only from the present x-ray scattering study.

VII. CONCLUSIONS

We have performed resonant x-ray scattering on DyB_2C_2 and have investigated the signals that correspond to the AFQ and AFM orders. The experimental results are analyzed both quantitatively and qualitatively using a theory of resonant x-ray scattering and a model of the AFQ order. An important result is that the quadrupolar order parameter manifests especially in the σ-σ' scattering which contains little magnetic contribution. We analyzed the resonant peak at (0 0 1/2) which corresponds to AFQ order using a parameter $d_2 = (f_{xx} - f_{yy})$ in this paper.

The (1̄ 0 1/2) reflection is also an important peak for a more detailed study of the AFQ order in this compound. One reason is that nonresonant σ-σ' scattering suggests a periodic displacement of the Dy ions below T_Q, which is probably caused by a quadrupole-strain coupling that is peculiar in this compound. Another reason is that a detailed investigation of the resonant peak could reveal the behavior of the canting angle of the moments especially in phase II, i.e., if it is zero or not. Both of these subjects require further studies.

We have also studied the critical phenomenon of AFQ ordering. The order parameter well follows a normal power law with a reasonable critical exponent for a 3D system. The second-order nature of the phase transition was confirmed from the continuous decrease of the order parameter and the diffuse scattering above T_Q.

Finally, although the intra-atomic d-f Coulomb interaction is expected to be the most probable origin of the anisotropic tensor of x-ray susceptibility in the $4f$-electron systems, we need further investigations, both theoretically and experimentally, to clarify the mechanism of the scattering process.

*Present address: Department of Physics, Tohoku University, Sendai, 980-8578, Japan.

†Present address: Department of Physics, Chiba University, Chiba, 263-8522, Japan.

‡Present address: Department of Applied Physics, University of Tokyo, Tokyo, 113-8656, Japan.

[1] P. M. Levy, P. Morin, and D. Schmitt, Phys. Rev. Lett. **42**, 1417 (1979).

[2] P. Morin and D. Schmitt, in *Ferromagnetic Materials*, edited by K. H. J. Buschow and E. P. Wohlfarth (Elsevier Science, Amsterdam, 1990), Vol. 5, p. 1.

[3] D. T. Keating, Phys. Rev. **178**, 732 (1969).

[4] M. Amara and P. Morin, J. Phys.: Condens. Matter **10**, 9875 (1998).

[5] M. Amara, R. M. Galéra, P. Morin, and J. F. Bérar, J. Phys.: Condens. Matter **10**, L743 (1998).

[6] M. Takata, E. Nishibori, K. Kato, M. Sakata, and Y. Moritomo, J. Phys. Soc. Jpn. **68**, 2190 (1999).

[7] Y. Ito and J. Akimitsu, J. Phys. Soc. Jpn. **40**, 1333 (1976).

[8] J. Akimitsu and Y. Ito, J. Phys. Soc. Jpn. **40**, 1621 (1976).

[9] G. P. Felcher, G. H. Lander, T. Arai, S. K. Sinha, and F. H. Spedding, Phys. Rev. B **13**, 3034 (1976).

[10] W. A. C. Erkelens, L. P. Regnault, P. Burlet, J. Rossat-Mignot, S. Kunii, and T. Kasuya, J. Magn. Magn. Mater. **63&64**, 61 (1987).

[11] J. M. Effantin, J. Rossat-Mignot, P. Burlet, H. Bartholin, S. Kunii, and T. Kasuya, J. Magn. Magn. Mater. **47&48**, 145 (1985).

[12] P. Link, A. Gukasov, J.-M. Mignot, T. Matsumura, and T. Suzuki, Phys. Rev. Lett. **80**, 4779 (1998).

[13] P. Link, A. Gukasov, J.-M. Mignot, T. Matsumura, and T. Suzuki, Physica B **259-261**, 319 (1999).

[14] J.-M. Mignot, P. Link, A. Gukasov, T. Matsumura, and T. Suzuki, Physica B **281&282**, 470 (2000).

[15] R. Shiina, H. Shiba, and P. Thalmeier, J. Phys. Soc. Jpn. **66**, 1741 (1997).

[16] K. A. McEwen, U. Steigenberger, K. N. Clausen, J. Kulda, J.-G. Park, and M. B. Walker, J. Magn. Magn. Mater. **177-181**, 37 (1998).

[17] H. Nakao, K. Magishi, Y. Wakabayashi, Y. Murakami, K. Koyama, K. Hirota, Y. Endoh, and S. Kunii, J. Phys. Soc. Jpn. **70**, 1857 (2001).

[18] F. Yakhou, V. Plakhty, H. Suzuki, S. Gavrilov, P. Burlet, L. Paolasini, C. Vettier, and S. Kunii, Phys. Lett. A **285**, 191 (2001).

[19] Y. Murakami, H. Kawada, H. Kawata, M. Tanaka, T. Arima, Y. Moritomo, and Y. Tokura, Phys. Rev. Lett. **80**, 1932 (1998).

[20] Y. Murakami, J. P. Hill, D. Gibbs, M. Blume, I. Koyama, M. Tanaka, H. Kawata, T. Arima, Y. Tokura, K. Hirota, and Y. Endoh, Phys. Rev. Lett. **81**, 582 (1998).

[21] G. Helgesen, J. P. Hill, T. R. Thurston, D. Gibbs, J. Kwo, and M. Hong, Phys. Rev. B **50**, 2990 (1994).

[22] S. Ishihara and S. Maekawa, Phys. Rev. B **58**, 13 442 (1998).

[23] S. Ishihara and S. Maekawa, Phys. Rev. Lett. **80**, 3799 (1998).

[24] I. S. Elfimov, V. I. Anisimov, and G. A. Sawatzky, Phys. Rev. Lett. **82**, 4264 (1999).

[25] M. Benfatto, Y. Joly, and C. R. Natoli, Phys. Rev. Lett. **83**, 636 (1999).

[26] M. Takahashi, J. Igarashi, and P. Flude, J. Phys. Soc. Jpn. **68**, 2530 (1999).

[27] S. Ishihara and S. Maekawa, Phys. Rev. B **62**, R9252 (2000).

[28] M. Blume, in *Resonant Anomalous X-ray Scattering, Theory and Applications*, edited by G. Materlik, C. J. Sparks, and K. Fischer (Elsevier Science, Amsterdam, 1994), p. 495.

[29] M. Blume, J. Appl. Phys. **57**, 3615 (1985).

[30] H. Yamauchi, H. Onodera, K. Ohoyama, T. Onimaru, M. Kosaka, M. Ohashi, and Y. Yamaguchi, J. Phys. Soc. Jpn. **68**, 2057 (1999).

[31] K. Hirota, N. Oumi, T. Matsumura, H. Nakao, Y. Wakabayashi, Y. Murakami, and Y. Endoh, Phys. Rev. Lett. **84**, 2706 (2000).

[32] Y. Tanaka, T. Inami, T. Nakamura, H. Yamauchi, H. Onodera, K. Ohoyama, and Y. Yamaguchi, J. Phys.: Condens. Matter **11**, L505 (1999).

[33] K. Dumesnil, A. Stunault, Ph. Mangin, C. Vettier, D. Wermeille, N. Bernhoeft, S. Langridge, C. Dufour, and G. Marchal, Phys. Rev. B **58**, 3172 (1998).

[34] J. P. Hannon, G. T. Trammell, M. Blume, and D. Gibbs, Phys. Rev. Lett. **61**, 1245 (1988).

[35] J. C. Lang, G. Srajer, C. Detlefs, A. I. Goldman, H. König, X. Wang, B. N. Harmon, and R. W. McCallum, Phys. Rev. Lett. **74**, 4935 (1995).

[36] F. Bartolomé, J. M. Tonnerre, L. Séve, D. Raoux, J. Chaboy, L. M. García, M. Krisch, and C. C. Kao, Phys. Rev. Lett. **79**, 3775 (1997).

[37] E. D. Isaacs, D. B. McWhan, D. P. Siddons, J. B. Hastings, and D. Gibbs, Phys. Rev. B **40**, 9336 (1989).

[38] D. Gibbs, D. R. Harshman, E. D. Isaacs, D. B. McWhan, D. Mills, and C. Vettier, Phys. Rev. Lett. **61**, 1241 (1988).

[39] D. Gibbs, G. Grübel, D. R. Harshman, E. D. Isaacs, D. B. McWhan, D. Mills, and C. Vettier, Phys. Rev. B **43**, 5663 (1991).

[40] S. W. Lovesey and K. S. Knight, Phys. Rev. B **64**, 094 401 (2001).

[41] H. Yamauchi *et al.* (private communication).

[42] J. C. Le Guillou and J. Zinn-Justin, Phys. Rev. Lett. **39**, 95 (1977).

[43] J. Als-Nielsen, O. W. Dietrich, and L. Passell, Phys. Rev. B **14**, 4908 (1976).

[44] A. I. Goldman, K. Mohanty, G. Shirane, P. M. Horn, R. L. Greene, C. J. Peters, T. R. Thurston, and R. J. Birgeneau, Phys. Rev. B **36**, 5609 (1987).

[45] M. P. Schulhof, P. Heller, R. Nathans, and A. Linz, Phys. Rev. B **1**, 2304 (1970).

[46] T. R. Thurston, G. Helgesen, J. P. Hill, D. Gibbs, B. D. Gaulin, and P. J. Simpson, Phys. Rev. B **49**, 15 730 (1994).

[47] K. Hirota, J. P. Hill, S. M. Shapiro, G. Shirane, and Y. Fujii, Phys. Rev. B **52**, 13 195 (1995).